

Limited Range Fractality of Randomly Adsorbed Rods

Daniel A. Lidar (Hamburger)^{a,b*}, Ofer Biham^{a†} and David Avnir^{b,c,d‡}

^a *Racah Institute of Physics, The Hebrew University, Jerusalem 91904, Israel*

^b *Fritz Haber Center for Molecular Dynamics, The Hebrew University, Jerusalem 91904, Israel*

^c *Institute of Chemistry, The Hebrew University, Jerusalem 91904, Israel*

^d *Minerva Center for Computational Quantum Chemistry, The Hebrew University, Jerusalem 91904, Israel*

Multiple resolution analysis of two dimensional structures composed of randomly adsorbed penetrable rods, for densities below the percolation threshold, has been carried out using box-counting functions. It is found that at relevant resolutions, for box-sizes, r , between cutoffs given by the average rod length $\langle \ell \rangle$ and the average inter-rod distance r_1 , these systems exhibit apparent fractal behavior. It is shown that unlike the case of randomly distributed isotropic objects, the upper cutoff r_1 is not only a function of the coverage but also depends on the excluded volume, averaged over the orientational distribution. Moreover, the apparent fractal dimension also depends on the orientational distributions of the rods and decreases as it becomes more anisotropic. For box sizes smaller than $\langle \ell \rangle$ the box counting function is determined by the internal structure of the rods, whether simple or itself fractal. Two examples are considered – one of regular rods of one dimensional structure and rods which are trimmed into a Cantor set structure which are fractals themselves. The models examined are relevant to adsorption of linear molecules and fibers, liquid crystals, stress induced fractures and edge imperfections in metal catalysts. We thus obtain a distinction between two ranges of length scales: $r < \langle \ell \rangle$ where the internal structure of the adsorbed objects is probed, and $\langle \ell \rangle < r < r_1$ where their distribution is probed, both of which may exhibit fractal behavior. This distinction is relevant to the large class of systems which exhibit aggregation of a finite density of fractal-like clusters, which includes surface growth in molecular beam epitaxy and diffusion-limited-cluster-cluster-aggregation models.

I. INTRODUCTION

The structure, packing and phase transitions in media composed of rod-like particles are of great importance in a large variety of physical systems [1–5]. Such systems include liquid crystals [6], slip lines in stressed metals and rocks, line-fractures in catalysts [7–9], fibers in paper sheets [10,11], and rod-like metal particles [12,13]. Unlike systems composed of nearly isotropic particles, for rod-like particles the orientational distribution plays an important role in addition to the positional distribution [14]. Systems of adsorbed particles can be classified to ones of penetrable [15–17] vs. impenetrable particles [4,5,18,19]. In this paper we will focus on the case of penetrable rods.

Many of the systems of interest in this context are essentially two dimensional and can be studied by a model in which M penetrable rods are randomly distributed on a two dimensional surface of size $L \times L$. Each rod is of length ℓ and width w . The effective two dimensional coverage is given by $\eta_2 = \rho \cdot \ell w$, where $\rho = M/L^2$ is the rod density. It provides a measure of the fraction of the area which is covered by the rods, where the reduction due to overlaps is ignored. Clusters of overlapping rods start to form at low rod density and increase in size as the density increases. Systems of this type exhibit a percolation transition at rod density ρ_c , above which there is an cluster which spans across the entire system. The percolation transition for systems of rod-like particles has been studied extensively in recent years [14,16,17,20–24]. A criterion for the percolation density ρ_c was obtained and examined for a variety of systems with different distributions of rod sizes and orientations. According to this criterion, percolation for isotropically oriented and randomly distributed rods occurs at rod density $\rho_c \cong 1/A_{exc}$ [17]. Here A_{exc} is the excluded area for placement of the center of a rod given that it may not intersect a rod already on the surface. This area, averaged over the isotropic orientational distribution is [17]:

*URL: <http://www.fh.huji.ac.il/~dani>

†URL: <http://www.fiz.huji.ac.il/staff/acc/faculty/biham>

‡URL: <http://chem.ch.huji.ac.il/employee/avnir/iavnir.htm>

$$A_{exc} = 2\left(1 + \frac{4}{\pi^2}\right)w\ell + \frac{2}{\pi}(\ell^2 + w^2). \quad (1.1)$$

Note that, since the excluded area A_{exc} , is not simply related to the rod area $\ell \cdot w$, the percolation threshold cannot be expressed as a function of the coverage η_2 alone. This distinguishes the rods from isotropic objects such as disks for which the excluded area is related to the disk area by a constant factor [17]. This difference is especially important in the case of large aspect ratio of the rods. In particular, for $w = 0$, the coverage vanishes but the excluded area does not.

The properties of the infinite percolation cluster at the transition have been studied extensively for lattice systems as well as for continuous systems such the the ones considered here [25,26]. In particular, its fractal nature was established. The fractal dimension, which can be expressed in terms of other critical exponents was found to be universal [26,27]. Properties such as correlation functions and cluster size distributions were also examined [28–30]. In addition to percolation systems, spatial fractal structures have been observed in a great variety of systems in physics [31–36] and chemistry [37].

In this paper we perform multiple resolution analysis of systems composed of randomly adsorbed rods below the percolation threshold ρ_c . In many empirical systems of this type, where adsorption and aggregation processes take place, fractal structures appear over a range of length scales for densities below ρ_c [38]. Moreover, a broad spectrum of fractal dimensions has been observed experimentally in such systems. To gain a better understanding of empirical fractal structures composed of rod-like particles we study these structures using multi-scale analysis, based on the box-counting (BC) function. In this analysis we examine the fractal properties of the entire system rather than a particular cluster. This procedure is the one most commonly used in experimental studies of adsorption and aggregation phenomena. In our analysis, we concentrate on a range of rod densities below the percolation threshold, where the area fraction covered by the rods is small. We identify two ranges of length scales, in which the observed dimension of the system is different from the space dimension. For length scales larger than the typical rod length, the results resemble those obtained for randomly distributed spheres [39]. An apparent fractal behavior is observed within a range of length scales between the rod length and the average distance between adjacent rods, which can span up to two decades. However, as was found before in percolation systems, highly anisotropic particles exhibit new and important features which do not appear in the study of isotropic particles such as spheres. In particular, we observe that, unlike the case of spheres, the upper cutoff (and thus the range over which apparent fractal behavior appears) cannot be expressed in terms of the effective coverage alone, but also depends on the excluded area. Moreover, we find that the apparent fractal dimension (FD) depends on the orientational distribution and decreases as it becomes more anisotropic. For length scales below the rod length, the BC function is dominated by the structure of the single rod whether simple or itself fractal. The class of systems which exhibits these two ranges includes the broad class of systems in which fractal-like clusters are adsorbed on a surface. To examine the fractal properties of such systems we study a simple one dimensional model in which the randomly distributed objects are Cantor sets. The paper is organized as follows. The model of randomly distributed rods is introduced in Section II and the box-counting function is examined. Rods of zero width are studied in Section III, randomly distributed Cantor sets in Section IV and a summary is presented in Section V.

II. THE GENERAL MODEL OF RANDOMLY ADSORBED RODS

In this Section we study a rather general model in which M rectangular rods are randomly adsorbed on a square surface of area L^2 . They are adsorbed with no correlations and are allowed to overlap with each other. The lengths of the rods $0 < \ell_i < \ell_{max}$, $i = 1, \dots, M$ are independently picked from the distribution $P_\ell(\ell)$ and the widths $0 < w_i < w_{max}$, $i = 1, \dots, M$ are picked from the distribution $P_w(w)$. The orientations $0 < \theta_i < \pi$ are picked from the distribution $P_\theta(\theta)$.

In order to examine the apparent fractal nature of the resulting random structures we apply the BC procedure. In this procedure one partitions the surface into a grid of mesh size $r \cdot L$ ($0 < r < 1$) and counts the number of boxes, $N(r)$, intersected by at least one rod, as a function of r . An analytical solution for the BC function $N(r)$ will now be obtained, and its slope examined in the different domains.

Imagine the surface of area L^2 to be initially empty and arbitrarily choose one of the grid-boxes of size $r \cdot L$. Denote the excluded area for placement of the center of rod i , given that the rod may not intersect the chosen box, by $S_r(\ell_i, w_i, \theta_i)$. This area is shown shaded in Fig. 1(a). Simple geometrical arguments yield:

$$S_r(\ell_i, w_i, \theta_i) = (r \cdot L)^2 + \ell_i \cdot w_i + r \cdot L(\cos \theta_i + \sin \theta_i)(\ell_i + w_i). \quad (2.1)$$

The two-fold rotation symmetry of the rods indicates that the angles θ_i are distributed in the range $0 \leq \theta_i \leq \pi$. However, the four-fold symmetry of the box makes the problem invariant under the transformation $\theta \rightarrow \theta + \pi/2$.

Therefore, we can simplify the calculations by considering only the range $0 \leq \theta_i \leq \pi/2$ with no effect on the results. The angle and side-lengths distributions are thus normalized so that:

$$\begin{aligned} \int_0^{\pi/2} d\theta P_\theta(\theta) &= 1 \\ \int_0^{\ell_{max}} d\ell P_\ell(\ell) &= \int_0^{w_{max}} dw P_w(w) = 1. \end{aligned} \quad (2.2)$$

We denote quantities averaged with respect to these distributions by angular brackets: $\langle \dots \rangle$.

Following Ref. [15] we consider the probability q_1 for random placement of the first rod without intersecting the box. This probability, which is proportional to the free area, is given by: $q_1 = [L^2 - S_r(\ell_1, w_1, \theta_1)]/L^2$. The next rod is placed with new random angle and side-lengths, so that the probability for two successful placements is: $q_2 = [1 - S_r(\ell_1, w_1, \theta_1)/L^2][1 - S_r(\ell_2, w_2, \theta_2)/L^2]$. Clearly, $q_M = \prod_{i=1}^M [1 - S_r(\ell_i, w_i, \theta_i)/L^2]$ is the probability of placing M rods without intersection with the chosen box. Thus, the probability of at least one intersection after M placements is $p_M = 1 - q_M$. Since the total number of boxes is $1/r^2$, for a given realization of angles and side-lengths the expected number of intersected boxes is p_M/r^2 , or:

$$N_{\{\theta_i, \ell_i, w_i\}}(r) = \frac{1}{r^2} \left[1 - \prod_{i=1}^M \left(1 - \frac{S_r(\ell_i, w_i, \theta_i)}{L^2} \right) \right]. \quad (2.3)$$

This expression still has to be averaged over the side-lengths and angle ensembles:

$$\begin{aligned} N(r) &= \langle N_{\{\theta_i, \ell_i, w_i\}}(r) \rangle \\ &= \frac{1}{r^2} \left\{ 1 - \left[\int_0^{\pi/2} d\theta P(\theta) \int_0^{\ell_{max}} d\ell \int_0^{w_{max}} dw P_\ell(\ell) P_w(w) \left(1 - \frac{S_r(\ell, w, \theta)}{L^2} \right) \right]^M \right\}. \end{aligned} \quad (2.4)$$

where the last equality follows since the θ_i are independent, identically distributed random variables, and so are ℓ_i and w_i . Finally, using Eq. (2.1) this can be expressed in terms of averages:

$$N(r) = \frac{1}{r^2} \left\{ 1 - \left[1 - r^2 - \frac{\langle \ell \rangle \langle w \rangle}{L^2} - r \langle (\cos \theta + \sin \theta) \frac{\langle \ell \rangle + \langle w \rangle}{L} \right]^M \right\}. \quad (2.5)$$

This BC function contains the information required for the multi-scale analysis of the system. In order to proceed with the scaling analysis, we turn next to the identification of the cutoffs, which separate between length scales in which $N(r)$ is dominated by the distribution vs. the internal structure of the rods. These cutoffs are determined by the effective dimensions of the rods, when projected onto the grid of boxes. Now, for a given rod i , which is oriented at an angle θ_i , the average between the projections along the x and y axes (parallel to the box sides) is $\ell_i(\cos \theta_i + \sin \theta_i)/2$ for the length and $w_i(\cos \theta_i + \sin \theta_i)/2$ for the width [Fig. 1(b)]. To obtain the effective cutoff, this should be averaged over all angles and side-lengths. We thus expect to find cutoffs at:

$$\begin{aligned} r_0^\ell &= \langle \cos \theta + \sin \theta \rangle \frac{\langle \ell \rangle}{2L} \\ r_0^w &= \langle \cos \theta + \sin \theta \rangle \frac{\langle w \rangle}{2L} \end{aligned} \quad (2.6)$$

Unlike the lower cutoffs which are determined by the rod dimensions, the upper cutoff (r_1) is given by the average distance between adjacent rod sides [39]:

$$r_1 = \frac{1}{\sqrt{M}} - \langle \cos \theta + \sin \theta \rangle \frac{\langle \ell + w \rangle}{2L} \quad (2.7)$$

To gain insight into the behavior of Eq. (2.5) we display it in Fig. 2 for the case of a random distribution of identical rods of length $\ell = d_1$ and width $w = d_2$ ($d_1 \gg d_2$) with isotropic orientations. We chose the case of narrow rods, since virtually all of the experimentally relevant cases mentioned above, belong to this category. In the next section we return to analyze the non-isotropic and polydispersed cases. The non-trivial apparent fractal region, is clearly seen in Fig. 2, between the predicted cutoffs of $\log_{10}(r_0^\ell) = -4.2$ and $\log_{10}(r_1) = -1.5$. It is the range which is

typical to all (fractal) resolution analyses, and which we claim, reveals apparent fractality. The apparent FD for this region (see derivation below) is $D = 0.06$. In Fig. 2, all four different approximately straight line regions are clearly identified, corresponding to the presence of the three cutoffs. The range $r < r_0^w$, is usually uninteresting from the experimental point of view because it probes the structure of the building block itself. It has a -slope (dimension) of 2, namely the dimension of the underlying plane. When $r_0^w < r < r_0^\ell$, the resolution of observation is coarser, and the rods appear as one-dimensional objects, reflected in the -slope (dimension) of approximately 1. The width of this range depends on the aspect ratio of the rods and is approximately $\log_{10}(\langle \ell \rangle / \langle w \rangle)$ in decades.

Having the cut-offs at hand, we now perform a scaling analysis in the region between them. This will be done by applying the standard fractal procedure

$$\log_{10} N(r) \sim -D \cdot \log_{10}(r) \quad (2.8)$$

where D is the apparent fractal dimension (FD). As stated above, the range which has been the focus of attention is the one in between the cutoffs $r_0^\ell < r < r_1$. The apparent FD, given by the slope in this range, is a non-universal dimension, the magnitude of which depends on the coverage. In order to obtain expressions for the coverage dependence, it is convenient to define effective one dimensional (1D) and two dimensional (2D) coverages. The effective 2D coverage is

$$\eta_2 = M \frac{\langle \ell \rangle \langle w \rangle}{L^2}. \quad (2.9)$$

while the effective 1D coverage is

$$\eta_1 = \eta_1^\ell + \eta_1^w \quad (2.10)$$

where $\eta_1^\ell = \sqrt{M} r_0^\ell$ and $\eta_1^w = \sqrt{M} r_0^w$ (note that as the rod widths approach zero $\eta_1 \rightarrow \eta_1^\ell$). The significance of the effective 1D coverage is that it provides a unified measure of coverage which is independent of the space dimension.

The width of the apparent fractal range, can be estimated by $\Delta_e = \log_{10}(r_1) - \log_{10}(r_0^\ell)$. In the case of large aspect ratio ($\langle w \rangle \ll \langle \ell \rangle$):

$$\Delta_e = \lim_{\langle w \rangle / \langle \ell \rangle \rightarrow 0} (\log r_1 - \log r_0^\ell) \approx \log(1/\eta_1 - 1). \quad (2.11)$$

Since in the limit of large aspect ratio $\eta_1 \propto (\rho \cdot A_{exc})^{1/2}$ up to a factor of order 1, it is found, from the criterion of Ref. [17] ($\rho_c \cong 1/A_{exc}$) that the width Δ_e is nearly zero in the vicinity of the percolation threshold, and increases as the density decreases below this threshold. This estimate for Δ_e may seem to suggest that one can increase the scaling range at will by decreasing the coverage. However, in addition to the width of the range between the cutoffs, the quality of the linear fit within this range measured by the coefficient of determination R^2 should be considered. One can limit the range of linearity by imposing a lower bound on R^2 . Obviously, the range decreases as R^2 increases. We thus conclude that the two cutoffs limit the width of the linear range for high coverage while the R^2 criterion limits it for low coverage [see Ref. [39] and compare Figs. 3(a) and 3(b)]. The net result is that the range of scaling is in fact restricted to 1-2 decades.

The apparent dimension is found by calculating the logarithmic derivative of $N(r)$ at the estimated middle point of the linear range. This point is situated at: $r_m = \sqrt{r_1 \cdot r_0^\ell}$. Assuming $\langle w \rangle < \langle \ell \rangle$ this yields for the apparent FD, in the $M \rightarrow \infty$ limit and at constant coverage, the general equation:

$$D = \frac{d \log[N(r)]}{d \log(r)} \Big|_{r_m} = 2 \left[1 - \frac{(1 - \eta_1)\eta_1^\ell + \eta_1 \sqrt{(1 - \eta_1)\eta_1^\ell}}{\exp[\eta_1^\ell(1 - \eta_1) + 2\eta_1 \sqrt{(1 - \eta_1)\eta_1^\ell} + \eta_2] - 1} \right] \quad (2.12)$$

This general formula for the FD will be used in the analysis to follow. The effects of changing the coverage on the apparent dimension, are shown in the inset of Fig. 2 for $d_1/d_2 = 10^3$: the FD increases monotonically with coverage, but does not reach 2 for the relatively narrow rods considered.

The dimension of the rods themselves can also be obtained from the box counting function. In order to do so one needs to identify the appropriate length scale and measure the slope of the box counting function $N(r)$ on the log – log plot. This slope should be obtained for a length which is the geometrical average of the effective cutoffs associated with the average rod length $\langle \ell \rangle$ and width $\langle w \rangle$ according to $r = \sqrt{r_0^\ell \cdot r_0^w}$. In the zero-width rod limit $d_2/d_1 \rightarrow 0$ this dimension approaches 1. As we are focusing especially on the experimentally relevant case of narrow rods, and as it is evident from Eqs. (2.9), (2.10) that both the FD and the range Δ_e are only marginally dependent on the rod width, we consider in the next cases, for simplicity, rods with zero width.

III. APPLICATIONS TO RODS OF ZERO WIDTH

In the present Section we consider for simplicity the case of rods with zero width. Some comparisons with simulations will be presented, as well as applications of the general theory to specific distributions of interest.

A. Isotropically Oriented Identical Rods

As a first case for the zero-width rods, let us return to the previous example of identical rods with isotropic orientations and impose zero width ($w = 0$). For the isotropic [$P_\theta(\theta) = 2/\pi$], monodispersed [$P_\ell(\ell) = \delta(\ell - d)$] case, the BC function and FD for rods of length d and zero width follow directly from Eqs. (2.5), (2.12) respectively:

$$N(r) = \frac{1}{r^2} \left\{ 1 - \left[1 - r^2 - r \frac{4d}{\pi L} \right]^M \right\}, \quad (3.1)$$

$$D = 2 \left[1 - \frac{\eta_1^\ell (1 + \sqrt{(1 - \eta_1^\ell) \eta_1^\ell - \eta_1^\ell})}{\exp[\eta_1^\ell (1 + 2\sqrt{(1 - \eta_1^\ell) \eta_1^\ell - \eta_1^\ell})] - 1} \right]. \quad (3.2)$$

In Fig. 3 we present this analytical result for the rod-BC function along with numerical simulations, for two coverages. The agreement between theory and simulations is excellent over the entire range of box-sizes. The ranges of apparent fractality are brought in the insets; one would expect the wavy nature of the line at the lower coverage, to be smeared out by noise in typical experimental situations. Comparing to the BC function for finite-width rods, which appears in Fig. 2, one observes that, as expected, there are now only two cutoffs and correspondingly three (approximately) linear regions of slope ~ 1 , $D < 1$ and 2.

B. Anisotropically Oriented Identical Rods

Anisotropically oriented elongated particles appear in a wide variety of systems, notably in liquid crystals. In order to investigate the effect of anisotropy on the apparent fractal properties we consider here the following angular distribution, normalized for $0 \leq \theta \leq \pi/2$:

$$P(\theta) = \frac{2\Gamma(1+n)}{\sqrt{\pi}\Gamma(1/2+n)} (\cos \theta)^{2n}. \quad (3.3)$$

In the limit $n \rightarrow 0$ this corresponds to a uniformly random distribution, whereas for $n \rightarrow \infty$, to perfectly aligned rods. The rods are assumed to be of equal size d . The BC function can be found by calculating the angular averages of Eq. (2.5). Using the identities ($n > 0$):

$$\int_0^{\pi/2} d\theta \cos^{2n+1} \theta = \frac{\sqrt{\pi}\Gamma(1+n)}{2\Gamma(3/2+n)} \quad (3.4)$$

$$\int_0^{\pi/2} d\theta \cos^{2n} \theta \sin \theta = \frac{1}{1+2n}, \quad (3.5)$$

we find:

$$\gamma_n \equiv (\langle \cos \theta + \sin \theta \rangle) = \frac{\Gamma(1+n)}{\Gamma(1/2+n)} \left(\frac{\Gamma(1+n)}{\Gamma(3/2+n)} + \frac{2}{\sqrt{\pi}(1+2n)} \right). \quad (3.6)$$

This yields for the BC function:

$$N(r) = \frac{1}{r^2} \left\{ 1 - \left[1 - r^2 - r \frac{d}{L} \gamma_n \right]^M \right\}. \quad (3.7)$$

In the $n \rightarrow 0$ limit one retrieves the result for uniformly randomly oriented rods, Eq. (3.1), whereas for $n \rightarrow \infty$ one finds $N(r) = \{1 - [1 - r^2 - r d/L]^M\}/r^2$. For the cutoffs we have from Eq. (2.6):

$$\begin{aligned}
r_0 &= \gamma_n \frac{d}{2L} \\
r_1 &= \frac{1}{\sqrt{M}} - \gamma_n \frac{d}{2L},
\end{aligned}
\tag{3.8}$$

and for the coverage:

$$\eta_1^\ell = \sqrt{M} \gamma_n \frac{d}{2L}
\tag{3.9}$$

The FD for the present case is found by substituting η_1^ℓ from Eq. (3.9) in the general expression Eq. (2.12) and taking $\eta_2 = 0$. The effect on D of changing n at constant number and size of rods is shown in Fig. 4: the apparent FD decreases as the rods become more parallel, i.e., as they “cover space” less effectively. For isotropic objects we have shown that the apparent FD depends essentially only on the coverage [39]. As seen here, for anisotropic objects, the FD depends on an additional parameter (the degree of anisotropy). This feature may be relevant to many experimental systems which exhibit anisotropic distributions of rod-like particles, such as liquid crystals and paper fibers.

C. Polydispersed Rods

We will now explore the effects of polydispersivity in the rods size. In particular we will consider a power-law distribution of the rod lengths.

1. Model

In Ref. [39] a variety of narrow size distributions were examined. It was observed that such polydispersivity does not alter the basic observation of an apparent fractal regime between cutoffs. The apparent FD of the corresponding monodispersed distribution was only slightly modified. An important distribution function found in numerous experimental cases is the power-law distribution of sizes [40]. To obtain such a distribution we choose rod lengths from an iteratively constructed Cantor set, containing 2^n segments of length $3^{-n}L$ in the n^{th} iteration. Assuming rod lengths are chosen uniformly from among these segments, the probability of choosing a segment of length $3^{-n}L$ is $P(\ell/L = 3^{-n}) = 2^n/Z$, where $Z = \sum_{k=1}^{k_m} 2^k$, k_m being the maximal iteration number in the construction of the Cantor set. The average rod length ℓ is then given by:

$$\langle \ell \rangle = \sum_{k=1}^{k_m} \ell P(\ell/L = 3^{-k}) = \frac{1}{Z} \sum_{k=1}^{k_m} 2^k 3^{-k} L = \frac{1 - (2/3)^{k_m}}{2^{k_m} - 1} L.
\tag{3.10}$$

Expressed in terms of lengths one finds for the distribution:

$$P(\ell) = \frac{1}{Z} 2^{-\log(\ell/L)/\log(3)} = \frac{1}{Z} (\ell/L)^{-D_c} ; \quad D_c = \frac{\log(2)}{\log(3)},
\tag{3.11}$$

D_c being the FD of the Cantor set. Thus the length distribution indeed satisfies a power-law [41]. Note that $P(\ell)$ is a *discrete* distribution with allowed lengths of $\ell = 3^{-n}L$, and that $\langle \ell \rangle$, for example, would be different if ℓ could assume any value between $3^{-k_m}L$ and $L/3$.

2. Scaling Analysis for Power-Law Dispersed Rods

We assume that the rods are uniformly randomly oriented, so that $\langle \cos \theta + \sin \theta \rangle = 4/\pi$, $0 \leq \theta < \pi/2$. We thus have from Eq. (2.5):

$$N(r) = \frac{1}{r^2} \left\{ 1 - \left[1 - r^2 - r \frac{4 \langle \ell \rangle}{\pi L} \right]^M \right\}
\tag{3.12}$$

with $\langle \ell \rangle$ given by Eq. (3.10). As can be seen in Fig. 5, for as few as $M = 62$ rods, Eq. (3.12) is in good agreement with the simulation results for rods with a power-law distribution of lengths. Thus, we find that the BC function can be derived analytically for a power-law distribution of particle dimensions, and depends essentially only on the first moment of this distribution. The apparent FD can also be found as before, as the slope between cutoffs determined by the average rod length. From Eq. (2.6), one gets in the zero-width rod limit:

$$\begin{aligned} r_0 &= \frac{2 \langle \ell \rangle}{\pi L} \\ r_1 &= \frac{1}{\sqrt{M}} - \frac{2 \langle \ell \rangle}{\pi L}. \end{aligned} \quad (3.13)$$

The effective 1D coverage is now given by:

$$\eta_1^\ell = \sqrt{M} \frac{2 \langle \ell \rangle}{\pi L}. \quad (3.14)$$

The FD is found from Eq. (3.2), with the present η_1^ℓ . The prediction of this formula is compared in Fig. 5 with a linear regression in the range set exactly by the above cutoffs, and is in good agreement. Thus the FD is still determined essentially only by the 1D coverage. This is a non-trivial result, since a power-law distribution is poorly described by its mean, yet this is essentially the only distribution-related quantity needed to express the BC function. It can be understood intuitively as follows: since the BC function counts the total number of occupied boxes, it is approximately proportional to the total length of all rods. This quantity is well described by the number of rods times the average rod-length, namely the 1D coverage. In the next Section we consider the effect of endowing the rods with an internal (fractal) structure.

IV. RANDOMLY ADSORBED CANTOR-RODS

So far we have dealt with random distributions of objects which are not themselves fractals. This was reflected in the BC function at resolutions below the lower cutoff, by an integer slope. In this Section we consider a model of randomly deposited rods which are all Cantor sets of $FD=D_c$. A new feature expected in this case, is that for perfect (i.e., not truncated) Cantor sets, a *non-integer* slope of $-D_c$ should appear below the lower cutoff, in contrast to the cases considered so far. The main motivation for considering a model of Cantor-rods, however, is that it mimics a large class of experimental systems where a set of fractal objects is randomly adsorbed on a surface. For example, DLA-like clusters growing simultaneously from several nucleation centers [42] and cluster-cluster aggregation experiments [43]. In such systems we expect an interplay between the FD of the fractal objects and the apparent FD induced by randomness. In particular, it might be difficult to disentangle the respective slopes of the BC function if the objects are fractal over a small range.

For simplicity we will now consider the one dimensional case where M Cantor sets (rods) of total length d each, are deposited on a line of length L . As in Sec.III, let n denote the number of iterations in the construction of the Cantor sets. Thus there are 2^n segments of length 3^{-n} in each rod. As before, the rods are fully penetrable to each other. In order to find the BC function for the resulting set, we focus on a single, arbitrary box of length $r \cdot L$ and calculate the excluded length for placement of the center of a rod, the condition being that the rod does not overlap with the box.

Let $\Omega_k^{(n)}$ denote the excluded length for placement of a single n^{th} iteration Cantor-rod, when the box-length satisfies: $3^{-k-1}d < r \cdot L < 3^{-k}d$. To find this function, consider first the case $n = 0$, i.e., the case of gapless rods of length d . This is nothing but the 1D version of equi-sized rods considered in Sec.II, and the excluded length is clearly $\Omega_0^{(0)} = r \cdot L + d$. When $n = 1$ there is a gap of length $d/3$ and one must distinguish between the cases $r \cdot L > d/3$ and $r \cdot L < d/3$. In the former, the resolution of the boxes is insufficient to notice the presence of the gap, namely, if the box overlaps with the gap it necessarily touches at least one of the two rod-segments as well. In this case, therefore, the excluded length is again $\Omega_0^{(1)} = r \cdot L + d$. However, when $r \cdot L < d/3$ a new situation arises: the box can fully overlap with the gap. This is equivalent to having two rods of length $d/3$, each contributing $r \cdot L + d/3$ to the excluded length: $\Omega_1^{(1)} = 2(r \cdot L + d/3)$. When $n = 2$ there are gaps of length $d/3$ and $d/9$, so that three cases arise: (1) $r \cdot L > d/3$, (2) $d/9 < r \cdot L < d/3$, (3) $r \cdot L < d/9$. The first two do not differ from $n = 1$ since the boxes are not small enough to resolve the $d/9$ gaps: $\Omega_0^{(2)} = r \cdot L + d$, $\Omega_1^{(2)} = 2(r \cdot L + d/3)$. The third case is equivalent to having four rods of length $d/9$, each contributing an excluded length of $r \cdot L + d/9$: $\Omega_2^{(2)} = 4(r \cdot L + d/9)$. The general case should now be clear:

$$\Omega_k^{(n)} = \begin{cases} r \cdot L + d & : r > d/L \\ 2^k(r \cdot L + 3^{-k}d) & : 3^{-k-1}d/L < r < 3^{-k}d/L, 0 \leq k \leq n \\ 2^n(r \cdot L + 3^{-n}d) & : r < 3^{-n-1}d/L. \end{cases} \quad (4.1)$$

It is convenient to express the index k satisfying the constraint in Eq. (4.1) as:

$$k = \lfloor \frac{\log[d/(r \cdot L)]}{\log(3)} \rfloor \quad (4.2)$$

(where $\lfloor x \rfloor$ is the largest integer smaller than x). Now suppose r is given, choose an arbitrary box, and place a Cantor-rod at random on the line. The probability q_1 that the rod does not intersect the box is the relative available length, i.e., $q_1 = 1 - \Omega_k^{(n)}/L$. For M independently placed Cantor-rods the probability that none intersects the chosen box is $q_M = q_1^M$, and the probability of at least one intersection is: $p_M = 1 - q_M$. When multiplied by the total number of boxes ($1/r$), this yields the expected number of intersected boxes:

$$N(r) = \begin{cases} [1 - [1 - (r + d/L)]^M] / r & : r > d/L \\ [1 - [2^k(r + 3^{-k}d/L)]^M] / r & : r < d/L, 0 \leq k \leq n \\ [1 - [2^n(r + 3^{-n}d/L)]^M] / r & : r < d/L, k > n. \end{cases} \quad (4.3)$$

where k is given by Eq. (4.2). This expression for the BC function is plotted in Fig. 6 for fifth generation Cantor-rods. The remarkable feature in comparison with randomly positioned full rods is that the lower cutoff has shifted to the left, now reflecting the size of the smallest segment in the Cantor-rods. At smaller resolutions the boxes again “see” 1D objects and the slope of the BC function is -1 . At a resolution of $r = d/L$ (rod-size), there is a smooth transition into the regime of apparent fractality associated with the random distribution of Cantor-rods. We believe that such behavior is typical of experimental situations where a random distribution of limited-range fractal objects is observed. However, unlike the present “clean” case, it may be much more difficult to separate the two regions in actual experimental data.

It should further be remarked that as can easily be checked, Eq. (4.3) yields a logarithmic derivative for $N(r)$ of $-D_c$ in the limits $n \rightarrow \infty$ and $r \rightarrow 0$. This implies the interesting result that regardless of coverage, a random ensemble of Cantor sets has exactly the same FD as a single Cantor set. Fig. 6 shows that in the range between the size of the smallest segment and the size of the set, the same conclusion holds for truncated Cantor sets. Clearly, our methods of calculation can be extended to other iteratively constructed fractal sets, and the conclusions above regarding the FD should therefore remain valid in such cases. We conjecture that they remain valid also for non-iteratively constructed fractals.

V. SUMMARY

We have performed a multiple resolution analysis using box counting functions to structures composed of randomly adsorbed rods. Such structures appear in a large variety of adsorption phenomena and in many physical systems including liquid crystals, aggregates of linear molecules and fibers and line fractures. The scaling properties of these systems are determined by the particle size (length and width) distribution, orientation distribution, as well as by correlations in the positions and orientations. In processes such as paper fiber sedimentation particles tend to aggregate into dense regions and create inhomogeneities [10,11]. In other systems, rods cannot overlap giving rise to a maximal jamming density [3,4].

We have studied the case where rods can overlap and there are no positional or orientational correlations between them. We examined various size distributions and orientation distributions, found an analytical expression for the box counting function and compared the analytical results to numerical simulations.

For rod densities below the percolation threshold, we identified two interesting ranges of length-scales in which the box counting analysis gives rise to non trivial scaling properties. In the range of length scales between the typical rod length and the typical distance between adjacent rods, the box counting function is determined by the positional and orientational distribution of the rods in the plane rather than the structure of the single rod. This gives rise to an apparent fractal behavior over a finite range of up to two decades. Unlike the case of randomly distributed isotropic objects (disks), the range of length scales over which apparent fractal behavior is observed depends not only on effective coverage but also on the excluded area (averaged over the orientational distribution). Moreover, the apparent fractal dimension depends on the orientational distribution and decreases as it becomes more anisotropic.

For length scales smaller than the typical rod length, the box counting function is determined by the internal structure of the rod. In case of ordinary one dimensional rods this gives rise to a dimension of 1. However, this result is more general and in case that the rods are trimmed into Cantor sets the FD which is observed in this range is equal to the FD of the single Cantor set. The distinction between these two ranges of length scales applies for a very broad class of systems which exhibit nucleation of a finite density of fractal-like clusters. The majority of spatial fractals in the physics literature belong to this class [38]. A finite density of fractal-like clusters appears in models such as diffusion-limited-cluster-cluster-aggregation [43] and in experimental systems such as molecular beam epitaxy where diffusion-limited-aggregation-like clusters nucleate at a finite density [42]. In these systems the fractal-like structure of the clusters results from complex stochastic dynamics. The cluster density is determined by parameters such as the temperature and deposition rate. The typical distribution is not exactly Poissonian due to effective repulsion between clusters. However, the distinction, emphasized here, between smaller length scales where the fractal properties are dominated by the single cluster and larger length scales where the distribution is dominant still applies. We thus predict that experiments involving random distributions of fractal-like objects, will reveal a cross-over from object-dominated to distribution-dominated fractal behavior.

ACKNOWLEDGMENTS

We would like to thank Prof. R.B. Gerber and D. Thimor for very helpful discussions. This work was supported by a grant from the Volkswagen Foundation, administered by the Niedersachsen Science Ministry. D.A. acknowledges support by the German BMBF and the Minerva Foundation, Munich.

-
- [1] L. Onsager, Ann. NY Acad. Sci. **51**, 627 (1949).
 - [2] P.J. Flory, Proc. Roy. Soc. London A **234**, 73 (1956).
 - [3] L. A. Chick and C. Viney, Molec. Cryst. Liq. Cryst. **226**, 25 (1993).
 - [4] P. Viot, G. Tarjus, S.M. Ricci and J. Talbot, J. Chem. Phys. **97**, 5212 (1992).
 - [5] S.M. Ricci, J. Talbot, G. Tarjus and P. Viot, J. Chem. Phys. **97**, 5219 (1992).
 - [6] P.-G. de Gennes, *The Physics of Liquid Crystals* (Clarendon Press, Oxford, 1974).
 - [7] N. Jost and E. Hornbogen, Pract. Met. **25**, 157 (1988).
 - [8] D. Romeu, A. Gomez, J.G. Perez-Ramirez, R. Silva, O.L. Perez, A.E. Gonzales and M.J. Yacaman, Phys. Rev. Lett. **57**, 2552 (1986).
 - [9] B.B. Mandelbrot, D.E. Passoja and A.J. Paullay, Nature **308**, 721 (1984).
 - [10] N. Provatas, T. Ala-Nissila and M.J. Alava, Phys. Rev. Lett. **75**, 3556 (1995).
 - [11] N. Provatas, M.J. Alava and T. Ala-Nissila, Phys. Rev. E **75**, 36 (1996).
 - [12] J.-Z. Zhang and D. Liu, J. Mater. Sci. **27**, 4329 (1992).
 - [13] R. Brunner, S. Gall, W. Wilke and M. Zrinyi, Physica A **214**, 153 (1995).
 - [14] I. Balberg and N. Binenbaum, Phys. Rev. B **28**, 3799 (1983).
 - [15] S. Torquato, G. Stell, J. Chem. Phys. **79**, 1505 (1983).
 - [16] G.E. Pike and C.H. Seager, Phys. Rev. B **10**, 1421 (1974).
 - [17] I. Balberg, C.H. Anderson, S. Alexander and N. Wagner, Phys. Rev. B **30**, 3933 (1984).
 - [18] S. Torquato, G. Stell, J. Chem. Phys. **78**, 3262 (1983).
 - [19] J.W. Evans, Rev. Mod. Phys. **65**, 1281 (1993).
 - [20] I. Balberg, N. Binenbaum and N. Wagner, Phys. Rev. Lett. **52**, 1465 (1984).
 - [21] A.L.R. Bug, S.A. Safran and I. Webman, Phys. Rev. Lett. **54**, 1412 (1985).
 - [22] I. Balberg, Phil. Mag. B **56**, 991 (1987).
 - [23] U. Alon, A. Drory and I. Balberg, Phys. Rev. A **42**, 4634 (1990).
 - [24] U. Alon, I. Balberg and A. Drory, Phys. Rev. Lett. **66**, 2879 (1991).
 - [25] D. Stauffer, *Introduction to Percolation Theory* (Taylor and Francis, London, 1985).
 - [26] M.B. Isichenko, Rev. Mod. Phys. **64**, 961 (1992).
 - [27] A. Kapitulnik, Y. Gefen and A. Aharony, J. Stat. Phys. **36**, 807 (1984).
 - [28] S. Torquato, J.D. Beasley and Y.C. Chiew, J. Chem. Phys. **88**, 6540 (1988).
 - [29] S.B. Lee and S. Torquato, J. Chem. Phys. **89**, 6427 (1988).
 - [30] S.B. Lee and S. Torquato, J. Chem. Phys. **91**, 1173 (1989).
 - [31] B. B. Mandelbrot, *The Fractal Geometry of Nature* (Freeman, San Francisco, 1982).

- [32] *On Growth and Form*, No. 100 in *NATO ASI Ser. E*, edited by H. E. Stanley, N. Ostrowsky (Martinus Nijhoff, Dordrecht, 1986).
- [33] *Fractals in Physics, Essays in Honour of B.B. Mandelbrot*, edited by J. Feder and A. Aharony (North Holland, Amsterdam, 1990).
- [34] H. Takayasu, *Fractals in the Physical Sciences* (J. Wiley & Sons, Chichester, 1990).
- [35] *Fractals in Science*, edited by A. Bunde, S. Havlin (Springer, Berlin, 1994).
- [36] A.-L. Barabási and H.E. Stanley, *Fractal Concepts in Surface Growth* (Cambridge University Press, Cambridge, 1995).
- [37] *The Fractal Approach to Heterogeneous Chemistry: Surfaces, Colloids, Polymers*, edited by D. Avnir (John Wiley & Sons Ltd., Chichester, 1992).
- [38] D.A. Lidar (Hamburger), O. Malcai, O. Biham and D. Avnir, in “Fractals and Chaos in Chemical Engineering”, World Scientific, Singapore (1996).
- [39] D.A. Hamburger, O. Biham and D. Avnir, *Phys. Rev. E* **53**, 3342 (1996).
- [40] Power law distributions appear in a large variety of physical systems and phenomena. A few examples are turbulence, $1/f$ noise, earthquakes and meteorite size distributions. See e.g. M. Schroeder, *Fractals, Chaos, Power Laws* (Freeman, New York, 1991) and references therein.
- [41] It is also a hyperbolic distribution [31], in the sense that $P(l/L \geq \lambda) = 2(\lambda^{-D_c} - 1)/Z \sim \lambda^{-D_c}$. This follows from $P(l/L \geq 3^{-n}) = \sum_{i=0}^{n-1} P(l = 3^{i-n}) = \sum_{i=0}^{n-1} 2^{n-i}/Z = 2(2^n - 1)/Z$ and $\lambda = 3^{-n}$.
- [42] R.Q. Hwang, J. Schröder, C. Gunther and R.J. Behm, *Phys. Rev. Lett.* **67**, 3279 (1991).
- [43] P. Meakin, in *Phase Transitions and Critical Phenomena, Vol. 12*, edited by C. Domb and J. L. Lebowitz (Academic Press, London, 1988), p. 335.

FIG. 1. (a) Excluded area for the placement of the center of a rod of length $\ell = d_1$ and width $w = d_2$ inclined at angle θ relative to the horizontal axis. If the center falls outside the shaded area, the rod will not intersect the box of side r ; (b) At the orientation shown, the projections of the sides, d_1 and d_2 , on the horizontal axis are $d_1 \cos \theta$ and $d_2 \sin \theta$ respectively (the sum of the two projections is shown by the thick line). The projections on the vertical axis are $d_1 \sin \theta$ and $d_2 \cos \theta$ respectively. Averaging over the two possibilities and θ yields Eq. (2.6).

FIG. 2. The BC function for rods (Eq. 2.5). Four approximately linear regimes indicate the presence of three cutoffs. As can be seen, the locations of these match the prediction of Eq. (2.6) [$\log_{10}(r_0^\ell) = -4.2$, $\log_{10}(r_0^w) = -7.2$, and $\log_{10}(r_1) = -1.5$]. The inset shows the apparent fractal dimension D , given by Eq. (2.12), (for the range of length scales between r_0^ℓ and r_1) plotted as a function of the effective 1D coverage η_1 . D increases monotonically with η_1 .

FIG. 3. BC functions for zero-width rods. (a) $\eta_1^\ell = 0.1$, $d_1 = 0.01$; Upper inset: typical configuration of rods; Lower inset: zoom between cutoffs $\log(r_0) = -2.2$, $\log(r_1) = -1.2$. (b) $\eta_1^\ell = 0.01$, $d_1 = 0.001$; Inset: zoom with agreement on slope between Eq. (3.2) and the linear regression to 2 significant digits.

FIG. 4. Apparent FD as a function of anisotropy parameter n [Eqs. (3.2), (3.9)], at two different 1D coverages ($dM^{1/2}$). The FD decreases as the rods tend to be more parallel, and as the coverage becomes smaller.

FIG. 5. BC functions for isotropically oriented rods of zero width and a power law distribution of lengths. The coverage here is $\eta_1 = 0.1$, the average rod length is $\langle l \rangle = 0.02$, the number of rods is $M = 62$, and the number of possible sizes generated by Cantor set iterations is $k_m = 6$. The inset shows the zoom between cutoffs $\log_{10}(r_0) = -1.89$ and $\log_{10}(r_1) = -0.94$.

FIG. 6. BC function for a random distribution of Cantor-rods on the interval (thick dashed-dotted line). Comparisons to the result for full rods of the same total length (solid line) as well as for a single perfect Cantor set with $FD=D_c$ (dashed line) are shown. The four regions observed for the Cantor-rods are (from left to right) of slope -1 , slope $-D_c$ (which is the Cantor-set dimension determined by the internal structure of the rods), apparent FD (which is determined by the coverage and the distribution of rods), and slope -1 again. In this example there are $M = 1000$ Cantor rods of size $d = 10^{-5} \cdot L$ each and the number of iterations in the construction of each rod is $n = 5$.

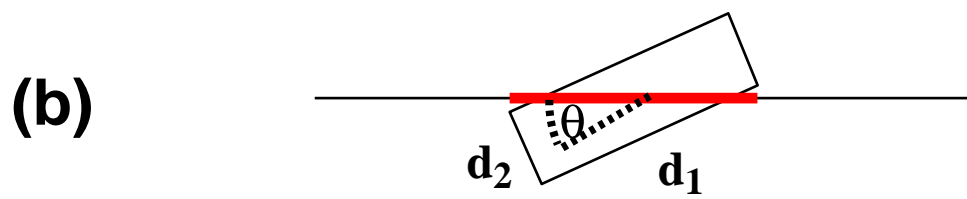
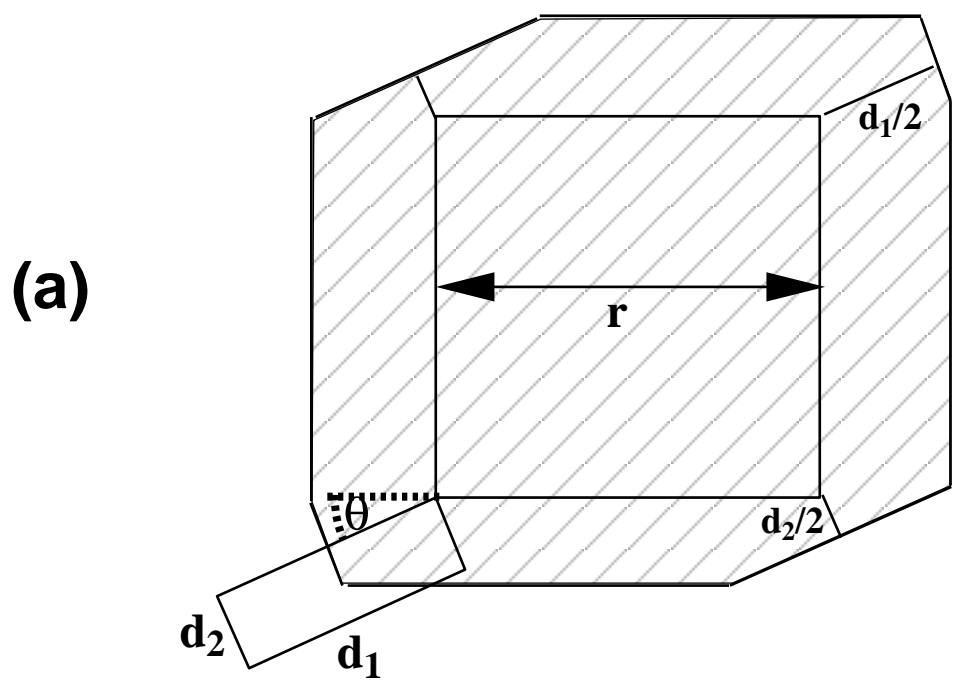


Fig. 1

$d_1=10^{-4}$, $d_2=10^{-7}$, $\eta_1=10^{-3}$, $M=985$

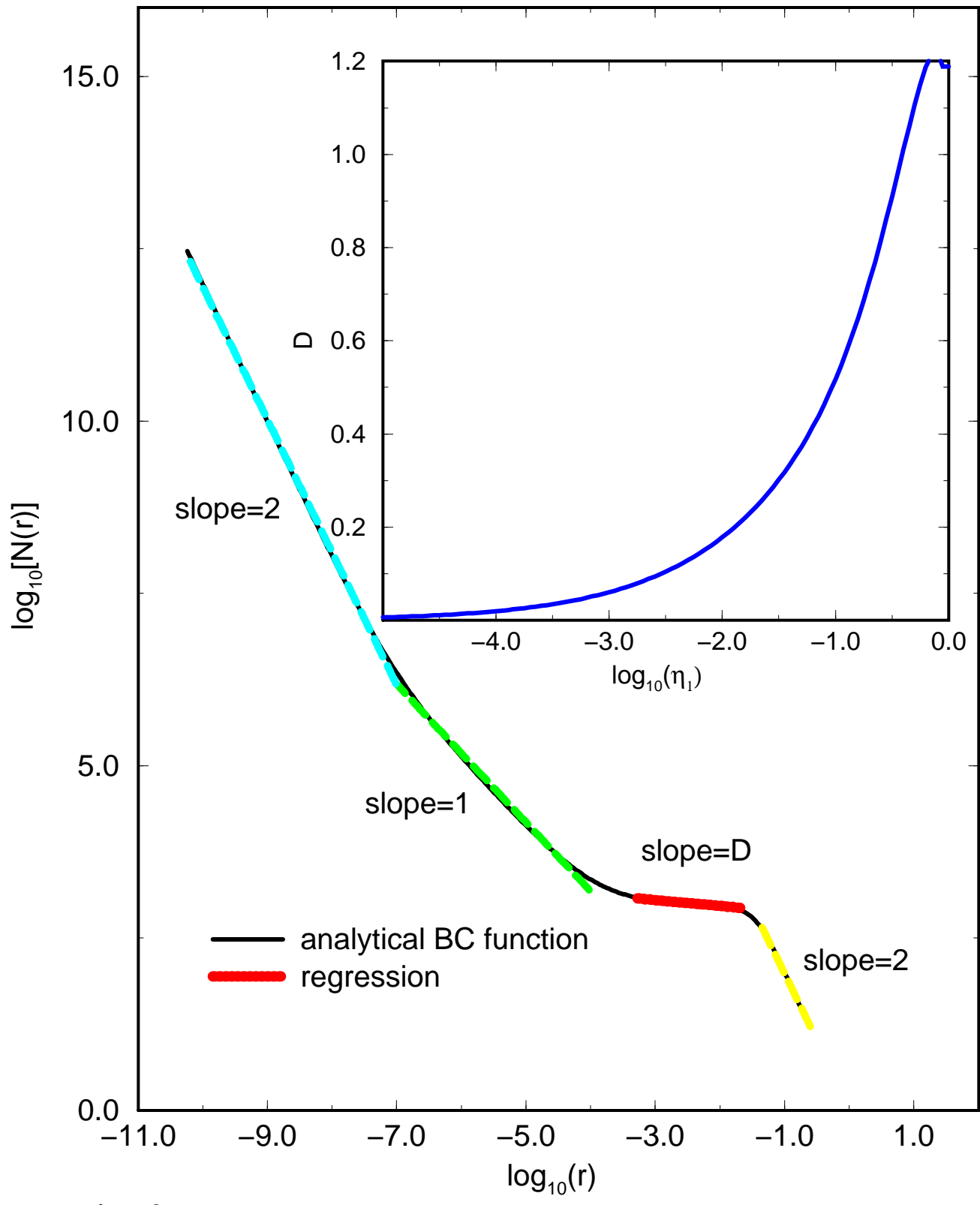


Fig. 2

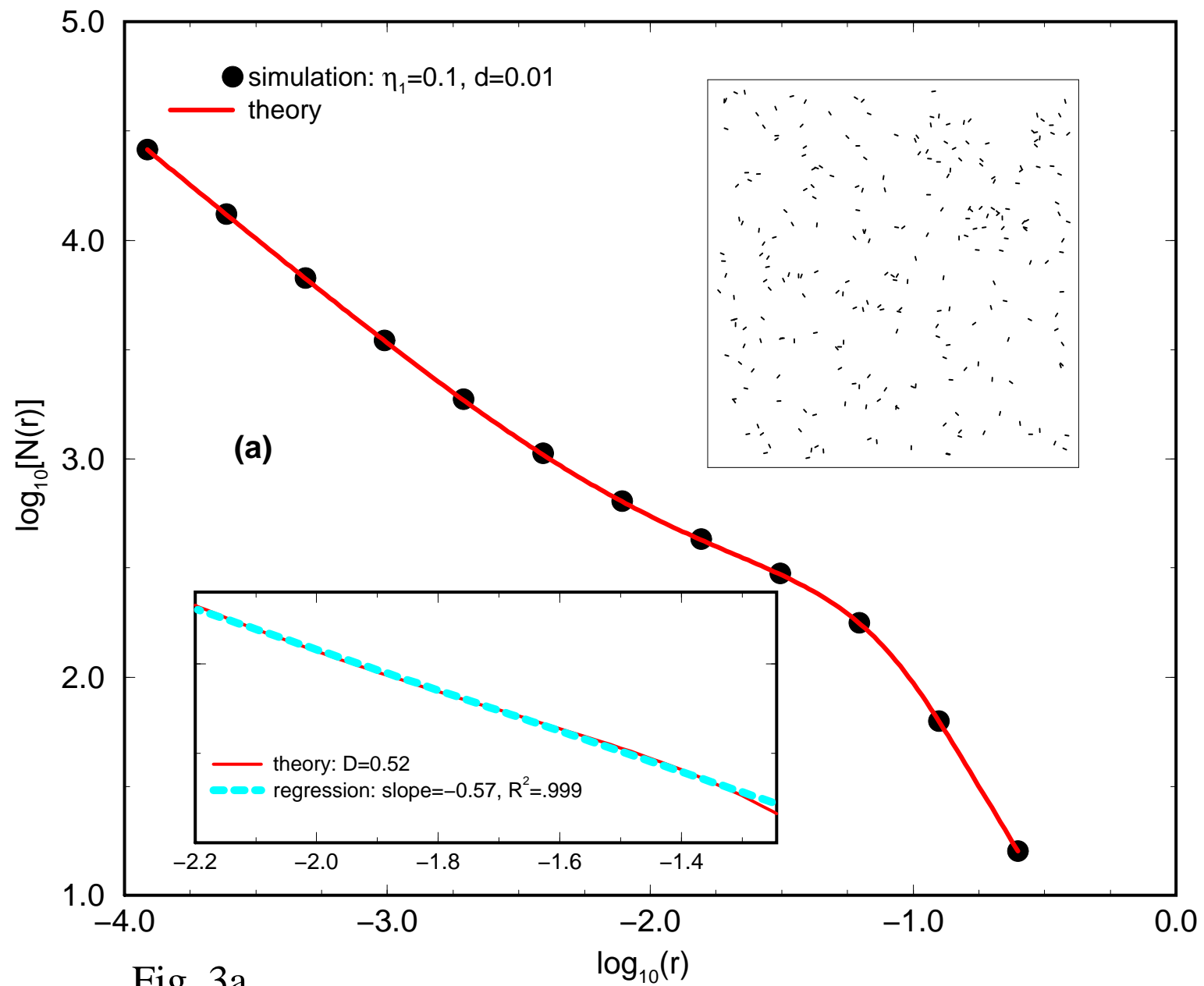


Fig. 3a

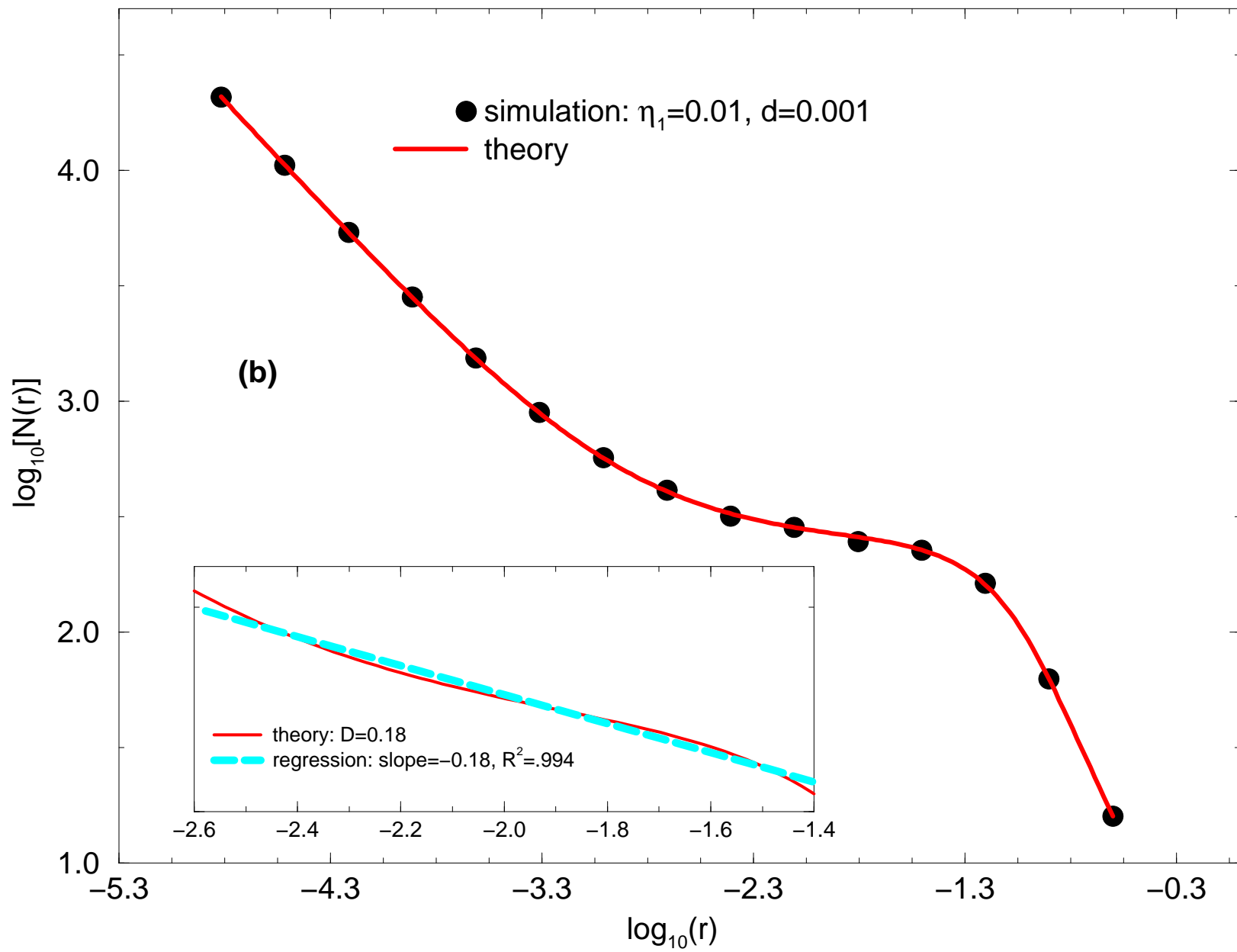


Fig. 3b

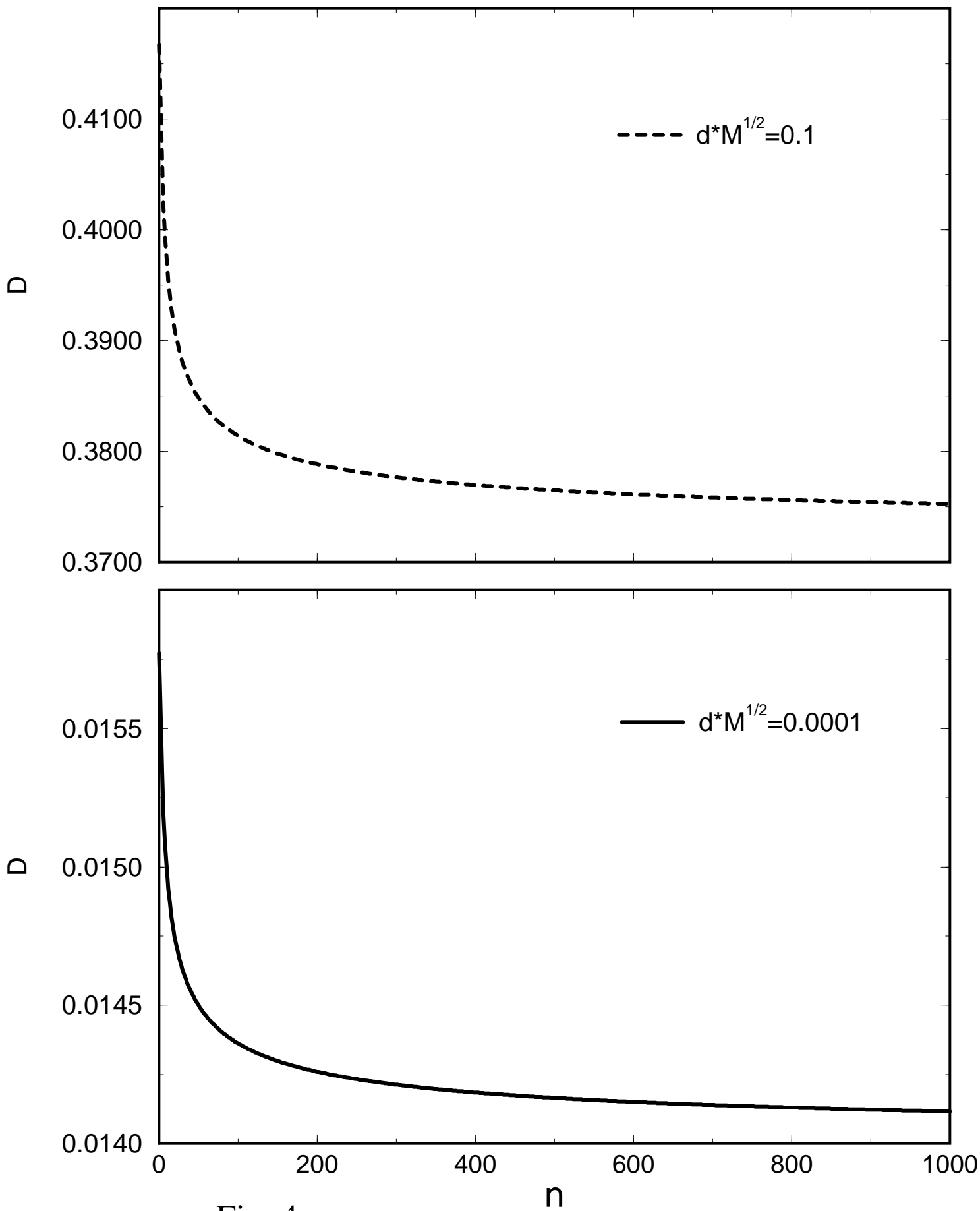


Fig. 4

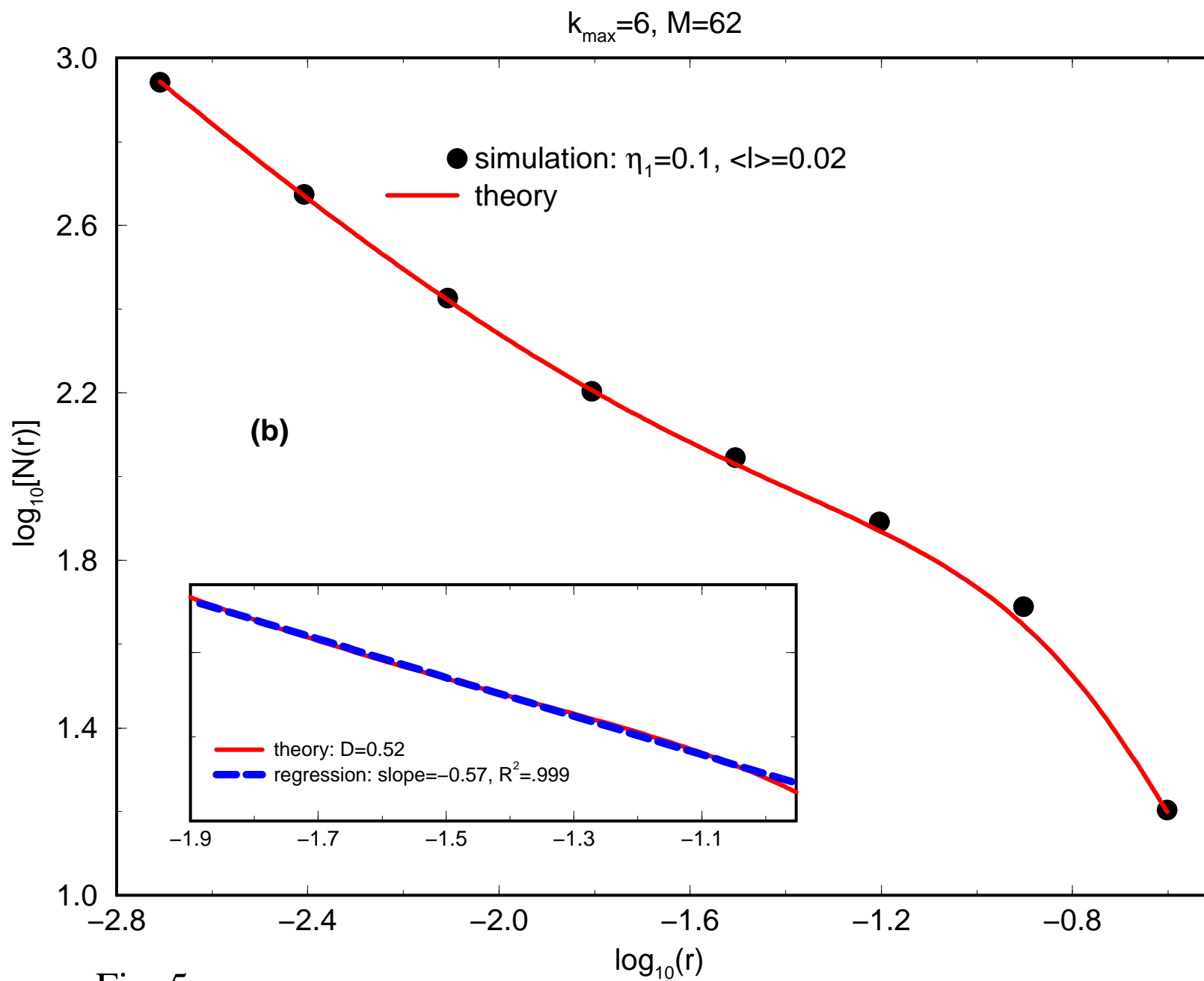


Fig. 5

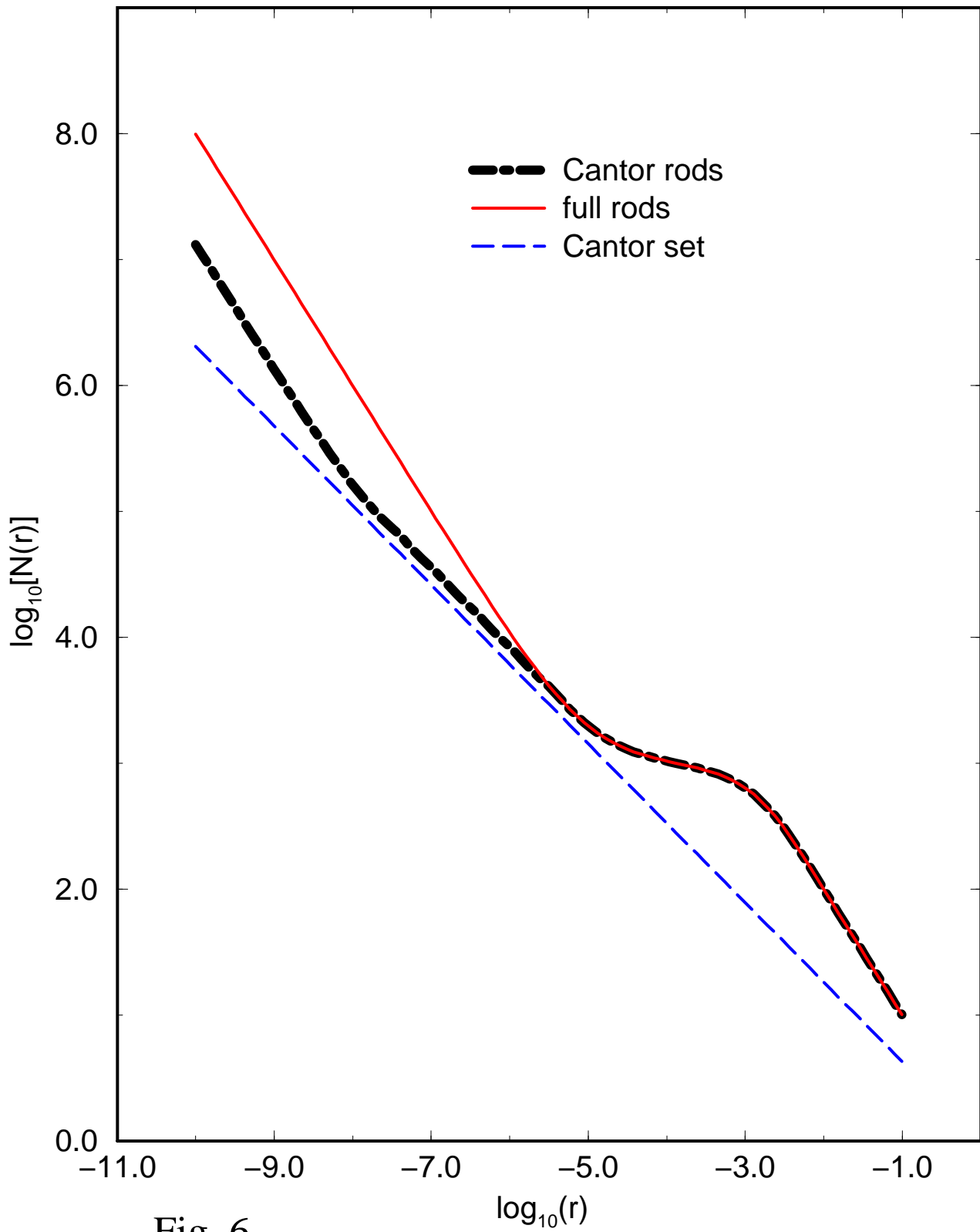


Fig. 6